IOP Publishing Journal of Physics: Condensed Matter
J. Phys.: Condens. Matter **31** (2019) 045001 (10pp) https://doi.org/10.1088/1361-648X/aaf0bf

Topological boundaries and bulk wavefunctions in the Su–Schreiffer–Heeger model

David S Simon[1,2], Shuto Osawa[2] and Alexander V Sergienko[2,3]

[1] Department of Physics and Astronomy, Stonehill College, 320 Washington Street, Easton, MA 02357, United States of America
[2] Department of Electrical and Computer Engineering & Photonics Center, Boston University, 8 Saint Mary's St., Boston, MA 02215, United States of America
[3] Department of Physics, Boston University, 590 Commonwealth Ave., Boston, MA 02215, United States of America

E-mail: simond@bu.edu, sosawa@bu.edu and alexserg@bu.edu

Received 26 September 2018, revised 31 October 2018
Accepted for publication 14 November 2018
Published 13 December 2018

Abstract

Working in the context of the Su–Schreiffer–Heeger model, the effect of topological boundaries on the structure and properties of bulk position-space wavefunctions is studied for a particle undergoing a quantum walk in a one-dimensional lattice. In particular, we consider what happens when the wavefunction reaches a boundary at which the Hamiltonian changes suddenly from one topological phase to another and construct an exact solution for the wavefunction on both sides of the boundary. The reflection and transmission coefficients at the boundary are calculated as a function of the system's hopping parameters, and it is shown that for some parameter ranges the transmission coefficient can be made very small. Therefore, it is possible to arrange a high degree of bulk wavefunction localization within each topological region, a fact that has information processing applications. This 'topologically-assisted' suppression of transitions, although not of direct topological origin itself, exists because of the presence of an abrupt change in the properties of the Hamiltonian at the topological boundary. We give a quantitative examination of the reflection and transmission coefficients of incident waves at the boundary between regions of different winding number.

Keywords: topological states, scattering theory, SSH model, topological boundaries

(Some figures may appear in colour only in the online journal)

1. Introduction

The Su–Schreiffer–Heeger (SSH) model [1] was originally proposed as a model of electron behavior in polymers, but has become widely used as a simple model in which topological phase transitions may occur. The system is defined in terms of two parameters, w and v, representing hopping amplitudes between two distinct types of lattice sites. Each unit cell is formed by a pair of lattice sites, one of each type (figure 1). As the quasimomentum k varies across the full Brillouin zone, the Hamiltonian $\hat{H}$ traces out a closed curve in a two-dimensional (2D) space. When the parameters obey $v > w$ this curve avoids enclosing the origin, where $\hat{H}$ becomes singular, and so the Hamiltonian exhibits a vanishing winding number about the singularity [2–4]. For $v < w$, the curve encloses the singular point, and has winding number 1 about the origin. At the borderline case $v = w$, a transition between two topological phases occurs, with the winding number making a discontinuous jump. Since the SSH lattice has two distinct sublattices, corresponding to two 'internal states' within each unit cell, the energies form two bands separated by a finite gap. However, when $v = w$, the gap disappears, and at this point transitions between different winding numbers occur.

In treatments of the SSH model, the emphasis is usually on the Hamiltonian and the energy bands. Wavefunctions are normally given less attention, and when they are discussed the

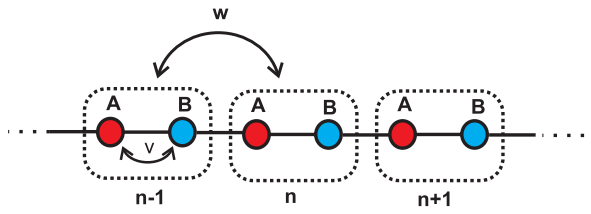

Figure 1. The SSH Hamiltonian describes motion of a particle hopping on a chain of sites with two substates per site. v and w are respectively the intracell and intercell hopping amplitudes per unit time.

focus is usually on Bloch states in momentum space or on the localized edge states that appear between regions of different winding number. However, recently the behavior of particles undergoing quantum walks in SSH-like systems has become an important topic of research; in particular photonic quantum walks in linear optical systems have been shown to simulate topological states of the same type that appear in SSH-like systems [4, 5, 6–10]. In these photonic systems, the particle is inserted at a fixed location, then at a later time (after some number of discrete time steps) its final position distribution is measured. Thus, position-space wavefunctions in the bulk are of significant interest and hold the key to a more complete understanding to transitions between topologically distinct regions.

Figure 2 shows a simulation of a photonic quantum walk. In (a), the entire system has the same Hamiltonian, and the photon spreads ballistically in both directions from the point of insertion, displaying the well-known probability distribution of quantum walk systems. However, in (b) the parameters of the system abruptly change at lattice site 85, causing the Hamiltonian on the right side of that point to have a different winding number than the Hamiltonian to the left. It can be clearly seen that penetration of the photon into the region on the right is strongly suppressed, with some of the amplitude collecting at the boundary and most of the rest reflecting back into the original region. Such a suppression of transitions into regions of different winding number may be seen in experimental data as well (see figure 3 of [8] for example), although in experiments the effect is often somewhat obscured due to the small number of steps measured and the presence of the localized state at the boundary that extends a few steps into the second region. Possibly because of these obscuring factors, this effect has not been much remarked upon. This reflection occurs even when there is no mismatch between energy levels on the two sides of the boundary.

Reflection occurs whenever there is an abrupt change in the wavefunctions across a boundary. This obviously occurs for sudden potential energy changes, but other sudden changes have similar effects, such as sudden changes in acoustic impedance or refractive index. Even sudden changes between regimes where relativistic dynamics and nonrelativistic dynamics dominate have been shown to lead to reflective behavior similar that at a potential step [13]. In this paper we show that abrupt changes in the topological state of the system are also typically accompanied by reflection and we give quantitative expressions for the resulting reflection and transmission coefficients for a specific model system.

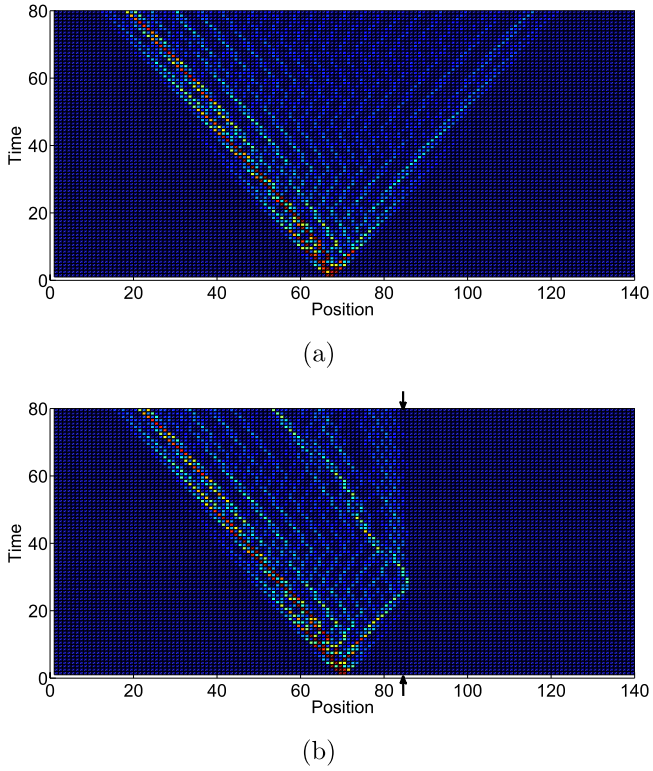

Figure 2. Calculated probability distribution of detecting a photon at position x at time t as the photon undergoes a one-dimensional (1D) quantum walk. The system in which the photon is walking is the linear optical arrangement of [11]. (a) The Hamiltonian is the same (of winding number zero) throughout. The photon is inserted into the system at position $x = 70$ and then exhibits the ballistic evolution characteristic of quantum walks. (b) The same, except that now the parameters of the system change at position $x = 85$ (marked by the arrows) so that the winding number of the Hamiltonian is 0 to the left of that point and 1 to the right. It can be seen that propagation into the region of 'wrong' winding number is strongly suppressed.

In particular, we look in detail at position-space wavefunctions of SSH systems and at what happens to them when the topology of the Hamiltonian changes. We assume that the Hamiltonian depends on some parameter that is under the control of experimenters (for example, the vertex phase parameters in the quantum walk systems of [10, 11] or the rotation angles of [4, 5, 6–8]). We further assume that the parameter varies in such a way that at some position x it causes the winding number of the Hamiltonian to change. Although all of the considerations in the following sections apply equally to other physical realizations, we will assume for the sake of specificity that the particles involved are photons.

In order to cross the boundary between the two regions the particle must make a transition between states that are asymptotically (far from the boundary) eigenstates of the original Hamiltonian to eigenstates of the topologically-altered Hamiltonian. We show in the following that if the two Hamiltonians are of different winding number, then such transitions are partially suppressed by an amount depending on the values of the v and w parameters of the two Hamiltonians, with strong reflection at the interface. The net result is that in a system of regions governed by Hamiltonians of different winding number, if the hopping amplitudes are

well-chosen, then states will strongly tend to remain in the region where they started and resist propagation into other regions. Although we have been speaking of spatial regions here, the same will apply to different regions of some more abstract parameter space: for example if a system is arranged such that photons see a polarization-dependent Hamiltonian that has different winding number for vertical and horizontal cases, then polarization flips will be suppressed by the same mechanism. This has obvious applications, for example in reducing the likelihood of polarization-flip errors in optical information processing systems. It is shown elsewhere [12] that Hamiltonians with such polarization-dependent winding numbers can be readily engineered using linear optics.

The existence of localized, topologically protected states at the boundaries between regions with different winding number is well-known. The results here imply that under appropriate conditions there is also a measure of approximate 'protection' attached to the bulk wavefunctions, in the sense that propagation into spatial regions or parameter regions with different topological properties is suppressed. The degree of transition suppression between these regions depends on the parameter values themselves, as well as the presence or absence of discrete topology changes. In this paper we only examine the simplest case, in which the two hopping parameters are interchanged at the boundary: the value of v on the left equals the value of w on the right, and vice-versa. A quantitative study of how the suppression varies as the values of v and w move away from the pure exchange case will be carried out elsewhere.

The quantum walk wavefunctions are linear combinations of energy eigenstates, so they do not strictly speaking have well-defined winding numbers of their own. But note that if one can strongly suppress transitions of the bulk wavefunction between regions of parameter space of different topology, one can associate the wavefunction localized in a given region with the winding number of the corresponding Hamiltonian. Then linear combinations of states associated to different winding number Hamiltonians may be formed, effectively forming qubits in a winding number basis:

$$a|0\rangle + b|1\rangle, \tag{1}$$

where $|0\rangle$ and $|1\rangle$ represent states associated with Hamiltonians of winding numbers 0 and 1. Such linear combinations can be easily arranged, for example, by inserting linear combinations of polarization states, with different polarizations being governed by Hamiltonians of different winding number. These qubits can be thought of as being encoded into either the Hamiltonian or into states present in the region governed by that Hamiltonian. Gates can then be made that act by altering the Hamiltonian, with readout accomplished by making measurements on the states.

In the coming sections, we will see that the presence of a change in the topology of the Hamiltonian (a discrete change in its winding number) affects the transmission and reflection coefficients at the boundary point. In the absence of the topology change, the transmission coefficient is uniformly equal to 100%. However, when the topology change is in place the transmission coefficient becomes a continuous function of the hopping parameters, and for some parameter ranges the transmission can be made very small.

This discussion points out that there can be interplay between discrete, topologically-based variables (winding number) and continuous variables (transmission coefficient) that interact with them. Such interplay exists in many other contexts. For example, the current across a Josephson junction is affected both by the existence of the topologically quantized, discrete magnetic flux and by the continuous temperature variable. In the case under discussion, changes in the discrete topological winding number and the continuous hopping parameters will both affect the behavior of other continuous variables associated with the same system, such as the reflection coefficient.

In this paper, we use the SSH system as an example system to study reflection and transmission at topological boundaries. In many applications of the SSH model, the electron or other hopping particle is treated as a point particle, perfectly localized at a given lattice site at each moment. In reality, we know that quantum mechanical wavefunctions typically have a finite spread to them and this spread needs to be taken into account to study quantities like scattering amplitudes and tunneling rates. In the current paper we are looking at the transition rate from one side of a discrete boundary to the other side, and this will clearly be dependent on the wave-like spatially-extended properties of the particle. So we focus on the position-space wavefunction and expand it in a convenient basis. In the context of a particle interacting with a discrete lattice system, a convenient basis is the Wannier basis, in which the wavefunction is built out of basis states that have finite spread but remain localized near the location of each lattice site. A particle initially localized near one site will exhibit a quantum walk [4, 14–16], evolving into a superposition of states localized at many sites; what we compute is the rate of transmission of this quantum walk state from one side of a topological boundary to the other.

The plan of the paper is as follows. In section 2 we briefly review the SSH model and set up the notation for what follows. In section 3 we construct the position- and momentum-space wavefuntions expressed in the Wannier basis. In section 4 we carry out a quantitative examination of reflection and transmission of the wavefunction at the boundary, making use of the transmission coefficient calculated explicitly in the appendix B. Finally, we summarize the results and discuss further aspects of them in section 5. Appendix A contains a brief description of two physical systems that can be used to simulate SSH behavior using photonic random walks.

Additional results related to the construction of edge and bulk wavefunctions in topological systems, complementary to those described here, have recently appeared in [17] and [18].

2. Brief review of SSH model

The SSH Hamiltonian [1] in one dimension describes the hopping of particles along the length of a bipartite lattice. A closely related model arose independently in quantum field theory [19].

The SSH system is shown schematically in figure 1. There is a lattice of unit cells, labeled by integer n, each of which

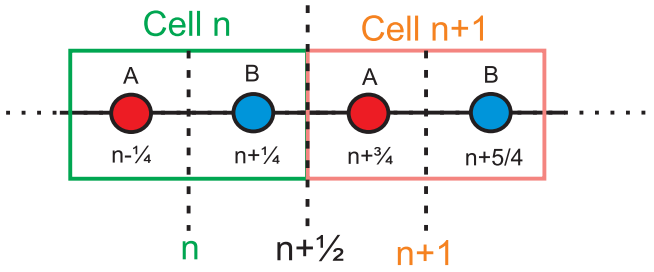

Figure 3. Two unit cells of the lattice. The coordinates are chosen so that the center of each cell is at an integer-valued location. The two subsites A and B are equally distant from the cell's center, so they are separated by half a unit, at locations $n \pm \frac{1}{4}$, for $n = 1, 2, \ldots, N$.

contains two subsites, denoted as A and B; these subsites represent two possible 'internal' states at cell n. There is an amplitude per unit time v to switch between the two states within the same cell, and an amplitude per time w to hop to an adjacent lattice site. Hopping to an adjacent site is always accompanied by a change of the internal state. By redefining the basis states if necessary, the hopping amplitudes v and w can always be chosen, without loss of generality, to be real.

Let R represent lattice positions and r be the position of the particle moving through the lattice. It is convenient to take the center of each unit cell to be at integer-valued positions, $R = n$, for $n = 1, 2, \ldots, N$, midway between the A and B subsites, as in figure 3. So the spacing between cells is one unit and the spacing between the A and B subsites within a cell is $1/2$ unit. Then the A subsites are at locations $n - \frac{1}{4}$ and the B sites are at $n + \frac{1}{4}$. In order to avoid edge effects, we may take periodic boundary conditions, so that site $n = N + 1$ is identified with site $n = 1$, or we may simply take N to be very large.

The position-space Hamiltonian is of the form:

$$\hat{H} = v \sum_{n=1}^{N} \left(|B,n\rangle\langle A,n| + |A,n\rangle\langle B,n| \right) + w \sum_{n=1}^{N-1} \left(|A,n+1\rangle\langle B,n| + |B,n\rangle\langle A,n+1| \right). \quad (2)$$

Here, $|A,n\rangle$, for example, denotes the state with a particle at site n in substate A.

At each fixed cell n or each fixed momentum k, this Hamiltonian is therefore a 2D matrix, and can be expanded in terms of the identity matrix and the Pauli matrices; for example, in momentum space one may write

$$\hat{H}(k) = d_0(k) I + \boldsymbol{d}(k) \cdot \boldsymbol{\sigma}. \quad (3)$$

This describes dynamics in a two-dimensional 'internal' subspace labeled by the two substates present at each lattice site. Generically, the two energy levels are separated by a k-dependent gap.

The Hamiltonian is completely characterized by the four-dimensional vector $\{d_0(k), \boldsymbol{d}(k)\}$. In the SSH model $d_0 = d_z = 0$, leaving $\boldsymbol{d}(k)$ confined to a plane. There is a singular point in this plane, at $\boldsymbol{d}(k) = 0$, where the phase of the Hamiltonian becomes indeterminate and the energy gap between bands vanishes. As k is varied across a full Brillouin zone, $\boldsymbol{d}(k)$ traces out a closed curve. These curves can be divided into two distinct classes: those that encircle the singular point and those that do not. In other words, those whose winding number about the origin is $\nu = 1$, and those of winding number $\nu = 0$. The winding number is highly stable in the sense that local perturbations causing continuous variations of the parameters cannot stimulate transitions between the discrete topological classes. Only a strong disturbance that alters the global structure of the system can cause the winding number to change.

In momentum space, the Hamiltonian is block diagonal, with blocks at each k value of the form

$$\hat{H}(k) = \begin{pmatrix} 0 & v + w\, \mathrm{e}^{-\mathrm{i}k} \\ v + w\, \mathrm{e}^{+\mathrm{i}k} & 0 \end{pmatrix} = \begin{pmatrix} 0 & z \\ z^* & 0 \end{pmatrix}, \quad (4)$$

where $z = v + w\, \mathrm{e}^{-\mathrm{i}k}$. The two dimensions of this matrix correspond to the two subsites A and B inside the unit cell.

An alternative form of this Hamiltonian will be useful. The off-diagonal terms can be written in polar form in the complex plane:

$$z = v + w\, \mathrm{e}^{-\mathrm{i}k} = \mathrm{e}^{-\mathrm{i}k/2} \left(v \mathrm{e}^{\mathrm{i}k/2} + w \mathrm{e}^{-\mathrm{i}k/2} \right) \quad (5)$$

$$= \mathrm{e}^{-\mathrm{i}k/2} \left((v+w) \cos\left(\frac{k}{2}\right) + \mathrm{i}(v-w) \sin\left(\frac{k}{2}\right) \right) \quad (6)$$

$$= \mathrm{e}^{-\mathrm{i}k/2} \left((v+w)^2 \cos^2\left(\frac{k}{2}\right) + (v-w)^2 \sin^2\left(\frac{k}{2}\right) \right)^{1/2} \mathrm{e}^{\mathrm{i}\theta_k} \quad (7)$$

$$= E_k \mathrm{e}^{\mathrm{i}\theta_k - \mathrm{i}k/2}, \quad (8)$$

where

$$E_k = \left((v+w)^2 \cos^2\left(\frac{k}{2}\right) + (v-w)^2 \sin^2\left(\frac{k}{2}\right) \right)^{1/2} \quad (9)$$

$$= \left(v^2 + w^2 + 2vw \cos k \right)^{1/2} \quad (10)$$

is the absolute value of z, while

$$\theta_k = \tan^{-1}\left(\frac{\mathrm{Im}(z)}{\mathrm{Re}(z)} \right) \quad (11)$$

$$= \tan^{-1}\left(\frac{(v-w)}{(v+w)} \tan\frac{k}{2} \right) \quad (12)$$

is the phase. So the Hamiltonian can be written as

$$H(k) = E_k \begin{pmatrix} 0 & \mathrm{e}^{\mathrm{i}\theta_k - \mathrm{i}k/2} \\ \mathrm{e}^{-\mathrm{i}\theta_k + \mathrm{i}k/2} & 0 \end{pmatrix}, \quad (13)$$

showing clearly the winding of H in the complex plane as the angle θ_k changes. The factor $\theta_k - \frac{k}{2}$ in the exponent is, up to a constant, a geometric Berry phase.

The eigenvalues are

$$E_\pm(k) = \pm E_k = \pm\sqrt{v^2 + w^2 + 2vw \cos k}. \quad (14)$$

It is then easy to verify that the eigenvectors are (up to an arbitrary overall phase):

$$|\pm\rangle = \frac{1}{\sqrt{2}}\begin{pmatrix} 1 \\ \pm e^{-i(\theta_k - \frac{k}{2})} \end{pmatrix} \equiv \frac{1}{\sqrt{2}}\begin{pmatrix} u_\pm \\ l_\pm \end{pmatrix}. \tag{15}$$

The upper component corresponds to the A substate, the lower to the B substate.

It should be kept in mind that the quasi-momentum k and the quasi-energy E are only defined modulo 2π.

3. Position-space wavefunctions

Ignoring for the moment the A and B subcells, consider a simple lattice with N sites at positions $R = 1, 2, \ldots, N$. One may construct the 1D Bloch wavefunctions for particle propagating through the lattice,

$$\psi_k(r) = e^{ikr} u_k(r), \tag{16}$$

where r is the particle position, and the allowed momenta are

$$k_n = \frac{2\pi n}{N} - \pi, \tag{17}$$

with $n = 1, \ldots, N$. We take the first Brillouin zone to run over the interval $-\pi < k \leqslant +\pi$. For a single k value, the corresponding position space wavefunction can be written in terms of the Wannier functions $\phi_R(r) = \phi(r - R)$ [20–22]:

$$u_k(r) = \frac{1}{\sqrt{N}} \sum_R e^{-ik(r-R)} \phi(r - R) \tag{18}$$

$$\psi_k(r) = e^{ikr} u_k(r) \; = \frac{1}{\sqrt{N}} \sum_R e^{ikR} \phi(r - R). \tag{19}$$

Wannier functions are widely used in solid state physics and other areas, and are defined as the Fourier transforms of the Bloch wavefunctions with respect to the discrete lattice positions,

$$\phi_R(r) = \phi(r - R) = \frac{1}{\sqrt{N}} \sum_k e^{-ikR} \psi_k(r). \tag{20}$$

There is one such function for each point in the crystal lattice and they are strongly localized near those lattice sites.

The functions centered at different lattice sites are orthogonal,

$$\int \phi^*(r - R)\phi(r - R')\mathrm{d}r = \delta(R - R'), \tag{21}$$

so the Wannier functions form a complete basis for spatial wavefunctions on the lattice. For the SSH model, these get multiplied by a 2D column matrix in the internal A/B space spanned by the two subsites at each n.

Now introduce the A and B sublattices, so that the lattice sites are shifted to $R = n \pm \frac{1}{4}$, where $n = 1, 2, \ldots, N$. This splits each term in the sum of equation (16) into two terms, one shifted the left by $\frac{1}{4}$ (the A terms) and the others shifting to the right by the same amount (the B terms), as in figure 3.

Because there are two substates at each unit cell, the energy splits into two bands, as in section 2. Taking into account that the $l_\pm$ and $u_\pm$ defined in equation (15) gain phases $\pm k/4$ from the shifts away from the cell center, the state then becomes

$$\psi_{k\pm}(r) = \frac{1}{\sqrt{2N}} \sum_{n=1}^{N} \left[\left(u_\pm e^{ik/4} \right) e^{ik(n-\frac{1}{4})} \phi\left(r - \left(n - \frac{1}{4} \right) \right) + \left(l_\pm e^{-ik/4} \right) e^{ik(n+\frac{1}{4})} \phi\left(r - \left(n + \frac{1}{4} \right) \right) \right] \tag{22}$$

$$= \frac{1}{\sqrt{2N}} \sum_{n=1}^{N} e^{ikn} \left[\phi\left(r - n + \frac{1}{4} \right) \pm e^{-i\theta_k + ik/2} \phi\left(r - n - \frac{1}{4} \right) \right], \tag{23}$$

where the $\pm$ labels correspond to the two eigenstates in the upper $(+)$ and lower $(-)$ bands. The first Wannier function inside the square bracket is centered at the A subsites, while the second function is localized near the B subsites.

Finally, the main interest here is not in wavefunctions of fixed k, but rather in states that are initially localized in position. Any position-space wavefunction at $t = 0$ can be expanded in terms of energy eigenstates,

$$\psi(r) = \sum_{k=1}^{N} \left(A_{k+} \psi_{k+}(r) + A_{k-} \psi_{k-}(r) \right). \tag{24}$$

The $A_{k\pm}$ coefficients can be found by taking the overlaps between $\psi(r)$ and the known initial wavefunction. There are two possibilities for the initial state: the photon may be inserted at an A subsite or a B subsite. In the first case, we take the initial state to be

$$\psi_A(r) = \phi\left(r - n_0 + \frac{1}{4} \right), \tag{25}$$

with n_0 being the label of the initial lattice site. In the latter case, we take the wavefunction to be

$$\psi_B(r) = \phi\left(r - n_0 - \frac{1}{4} \right). \tag{26}$$

Making use of the orthonormality of the Wannier functions, it is straightforward then to find that the wavefunctions at $t = 0$ for the two cases are

$$\psi_A(r) = \frac{1}{\sqrt{2N}} \sum_k e^{-ikn_0} \left(\psi_{k+}(r) + \psi_{k-}(r) \right) \tag{27}$$

$$\psi_B(r) = \frac{1}{\sqrt{2N}} \sum_k e^{-ikn_0} e^{+i(\theta_k - \frac{k}{2})} \left(\psi_{k+}(r) - \psi_{k-}(r) \right). \tag{28}$$

Clearly, the k values are uniformly distributed in probability, as would be expected for a wavefunction localized in space.

Again using the orthonormality of the Wannier functions, it follows readily that these initially-localized functions also form an orthonormal set:

$$\int \psi_A^*(r) \psi_A'(r) \, \mathrm{d}r = \delta(n_0' - n_0) \tag{29}$$

$$\int \psi_B^*(r)\psi_B'(r)\,\mathrm{d}r = \delta(n_0' - n_0) \tag{30}$$

$$\int \psi_B^*(r)\psi_A'(r)\,\mathrm{d}r = 0, \tag{31}$$

where n_0 and n_0 are the initial cells of the two wavefunctions.

All of the expressions above were at $t = 0$. Evolving forward in time, the energy eigenstates become

$$\psi_{k+}(r,t) = \mathrm{e}^{-\mathrm{i}E_k t}\psi_{k+}(r) \tag{32}$$

$$= \frac{1}{\sqrt{2N}}\sum_{n=1}^{N}\mathrm{e}^{\mathrm{i}(kn-E_k t)}\left[\phi\left(r-n+\frac{1}{4}\right) + \mathrm{e}^{-\mathrm{i}\theta_k+\mathrm{i}k/2}\phi\left(r-n-\frac{1}{4}\right)\right] \tag{33}$$

$$\psi_{k-}(r,t) = \mathrm{e}^{+\mathrm{i}E_k t}\psi_{k-}(r) \tag{34}$$

$$= \frac{1}{\sqrt{2N}}\sum_{n=1}^{N}\mathrm{e}^{\mathrm{i}(kn+E_k t)}\left[\phi\left(r-n+\frac{1}{4}\right) - \mathrm{e}^{-\mathrm{i}\theta_k+\mathrm{i}k/2}\phi\left(r-n-\frac{1}{4}\right)\right]. \tag{35}$$

This means that the A- and B-type wavefunctions become

$$\psi_A(r,t) = \frac{1}{N}\sum_{kn}\mathrm{e}^{\mathrm{i}k(n-n_0)}\left(\phi\left(r-n+\frac{1}{4}\right)\cos(E_k t) + \mathrm{i}\mathrm{e}^{-\mathrm{i}\theta_k+\mathrm{i}\frac{k}{2}}\phi\left(r-n-\frac{1}{4}\right)\sin(E_k t)\right) \tag{36}$$

$$\psi_B(r,t) = \frac{1}{N}\sum_{kn}\mathrm{e}^{\mathrm{i}k(n-n_0)}\left(\mathrm{i}\mathrm{e}^{\mathrm{i}\theta_k-\mathrm{i}\frac{k}{2}}\phi\left(r-n+\frac{1}{4}\right)\sin(E_k t) + \phi\left(r-n-\frac{1}{4}\right)\cos(E_k t)\right) \tag{37}$$

where t is an integer multiple of some discrete time interval T. Time evolution only alters the phase of each k component by a factor $\mathrm{e}^{\mathrm{i}E(k)t}$, and therefore the probability of finding each k value is constant in time. However interference between different terms in the sum leads to nontrivial time evolution for the spatial distribution.

Note that the factor of $\mathrm{e}^{\mathrm{i}(kn-E_k t)}$ in equation (33), which implies that the states ψ_{k+} on the positive-energy band are right-moving for positive k and left-moving for negative k. The negative-energy states ψ_{k-} move in the opposite direction: left for $k > 0$ and right for $k < 0$.

4. Transitions at topological boundaries

Recall that the topological sector of the system is determined by whether $v > w$ or $v < w$. Consider two sets of values of (v, w) and (v', w'), leading to two values of the phases, θ_k and θ_k', and corresponding wavefunctions $\psi_{k\pm}(r)$ and $\psi_{k\pm}'(r)$. These wavefunctions are eigenstates of Hamiltonians $\hat{H}(k)$ and $\hat{H}'(k)$. We take the full Hamiltonian of the system to be $H(k)$ for $n = -N+1, \ldots, 0$ and $H'(k)$ for $n = 1, \ldots, N$, where N is assumed large enough to ignore effects from the ends.

Now suppose that $\hat{H}(k)$ and $\hat{H}'(k)$ differ in winding number. Among other things, this implies that the signs of θ_k and θ_k' are opposite at the same value of k. We will restrict ourselves to the simplest case and assume that the initial and final hopping amplitudess are simply interchanged: $v' = w$ ands $w' = v$. In this case, we find that

$$\theta_k' = -\theta_k = +\theta_{-k}. \tag{38}$$

Referring to equation (23) and suppressing the time-dependent factors for simplicity, the energy eigenstates of H' can be written in terms of the phase θ_k of H as

$$\psi_{k\pm}'(r) = \frac{1}{\sqrt{2N}}\sum_{n=1}^{N}\mathrm{e}^{\mathrm{i}kn}\left[\phi\left(r-n+\frac{1}{4}\right) \pm \mathrm{e}^{+\mathrm{i}\theta_k-\mathrm{i}k/2}\phi\left(r-n-\frac{1}{4}\right)\right] \tag{39}$$

$$= \frac{1}{\sqrt{2N}}\sum_{n=1}^{N}\mathrm{e}^{\mathrm{i}(kn+\theta_k+k/2)}\left[\mathrm{e}^{-\mathrm{i}\theta_k-\mathrm{i}k/2}\phi\left(r-n+\frac{1}{4}\right) \pm \phi\left(r-n-\frac{1}{4}\right)\right]. \tag{40}$$

Now shift the origin by $\frac{1}{2}$ unit, $r \to r - \frac{1}{2}$, and shift the summation index $n \to n - 1$ in the second sum. After a few steps of algebra, one finds that the new wavefunctions are related to the old ones by

$$\psi_{k\pm}'(r) = \pm\mathrm{e}^{\mathrm{i}(\theta_k-\frac{3k}{2})}\psi_{k\pm}(r). \tag{41}$$

The phases linear in k come from the shifts in origin for r and n. The A and B wavefunctions are now

$$\psi_A'(r) = \frac{1}{\sqrt{2N}}\sum_{k}\mathrm{e}^{-\mathrm{i}kn_0}\mathrm{e}^{\mathrm{i}(\theta_k-\frac{3k}{2})}\left(\psi_{k+} - \psi_{k-}\right) \tag{42}$$

$$\psi_B'(r) = \frac{1}{\sqrt{2N}}\sum_{k}\mathrm{e}^{-\mathrm{i}k(n_0+2)}\left(\psi_{k+} + \psi_{k-}\right). \tag{43}$$

Aside from the extra phase factors, it can be seen that the change of winding number as the Hamiltonian changes from H to H' has effectively converted the A-type wavefunctions into B-type wavefunctions, and vice-versa.

The interchange of v and w essentially redefines the unit cells, shifting each cell by one-half unit. This interchanges the roles of the A and B subsites, as shown in figure 4. Moreover, as would be expected from a topological transition, the change from A being to the left of B within the unit cell to having A on the right is a *discrete* change, and this change must be carried out globally on the entire system.

In the case we consider ($v' = w$ and $w' = v$) it should be noted that the energy eigenvalues are the same on both sides of the boundary: $E_k = E_k'$, so any reflection at the boundary is not due to mismatch of energy levels. In fact, the total energy of the A and B modes vanishes on both sides. For example,

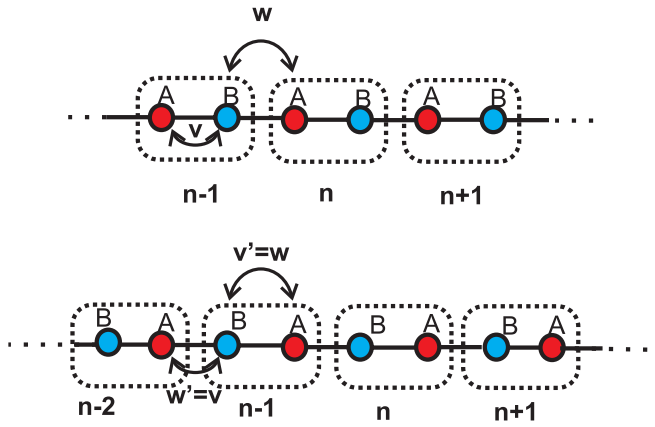

Figure 4. Interchanging v and w amounts to shifting the units cells by a distance of $\frac{1}{2}$ units, which effectively reverses the roles of A and B subsites. The top and bottom figures represent the two cases.

$$E_A = \langle\psi_A|\hat{H}|\psi_A\rangle \tag{44}$$

$$= \frac{1}{2N}\sum_{k,k'} e^{-i(k-k')n_0}\left[+E_k\left(\langle\psi_{k'+}|\psi_{k+}\rangle + \langle\psi_{k'-}|\psi_{k+}\rangle\right)\right. \tag{45}$$
$$\left. -E_k\left(\langle\psi_{k'+}|\psi_{k-}\rangle + \langle\psi_{k'-}|\psi_{k-}\rangle\right)\right]$$

$$= 0. \tag{46}$$

The vanishing of the energies makes intuitive sense: each A or B state is an equal superposition of eigenstates from the upper and lower bands. Since the energies of the two bands are negatives of each other, the total energy must be zero.

A more quantitative examination can be made of the transition across the boundary. We take the boundary to occur at the $n = 0$ cell, with the roles of v and w reversing once the B subsite of that cell is crossed. Only right-moving modes can cross from the left side to the right, so consider a positive-energy right-moving mode ($k > 0$) encountering the boundary; some of the amplitude can reflect to the left, some may be transmitted to the right. In addition, a localized edge state can be built up around the boundary. So one may consider a state of the form

$$|\Psi\rangle = |\psi_{k+}\rangle + r_k|\psi_{-k,+}\rangle + t_k|\psi'_{k+}\rangle + |\psi_{e,k}\rangle, \tag{47}$$

where the terms on the right represent the incident, reflected, transmitted, and edge states. (A similar state can be constructed using a right-moving negative energy state with $k < 0$; the results will be similar.) This state must satisfy the eigenvalue equation

$$\hat{H}|\Psi\rangle = E_k|\Psi\rangle. \tag{48}$$

Equation (48) can be solved exactly: the solutions for a_0, b_0, a_1, b_1, as well as for the reflection and transmission amplitudes r_k and t_k, are given in appendix B. For given values of v and w, the transmission probability at a fixed k value, $|t_k|$, peaks at $k = \frac{\pi}{2}$, dropping to zero at $k = 0, \pi$ (figure 5). When the two hopping amplitudes are equal, $v = w$, the transmission is 100%, as would be expected, since the two sides of the boundary are identical at this value. However, as the difference $|v - w|$ increases, the peak transmission drops (figure 6).

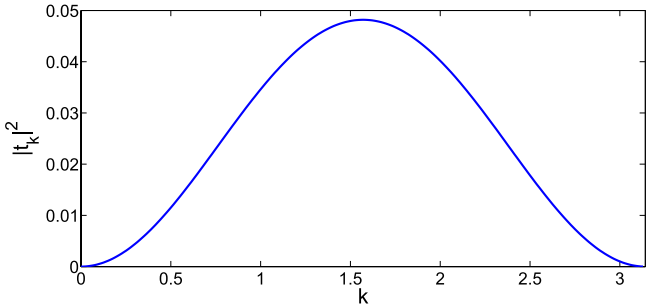

Figure 5. The transmission probability $|t_k|^2$ between the regions of different winding number always peaks at $k = \frac{\pi}{2}$, dropping to 0 at $k = 0, \pi$. The plot here is for $N = 500$, $v = 0.1$, and $w = 0.9$.

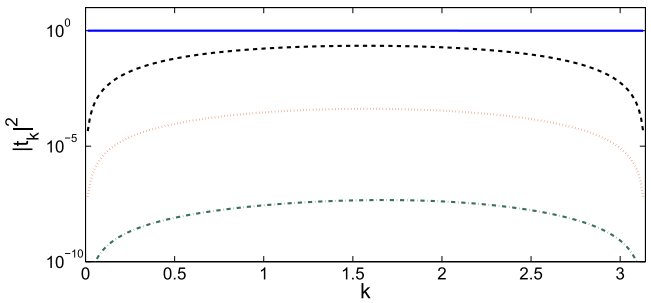

Figure 6. Logarithmic plot of transmission probability $|t_k|^2$ for several values of v and w. The transmission probability is constant at $|t_k|^2 = 1.0$ for $v = w$, but drops as $|v - w|$ increases. Increasing $|v - w|$ increases the value of $|\theta_k|$ at each nonzero k, leading to a larger phase shift at the boundary. The values plotted here are $(v, w) = (.5.5)$ (solid blue), $(.2, .8)$ (dashed black), $(.01, .99)$ (dotted red), and $(.001, .999)$ (dash-dot green). As $|v - w| \to 1$, the peak transmission $|t_k|^2 \to 0$.

We see then that by choosing w close to 0 and v close to 1, or vice versa, we can make the transmission of the wavefunction into the second region arbitrarily small, even though the energy levels are identical on both sides. A figure of merit might be taken to be

$$T_{\max} \equiv \max_k\left(|t_k|^2\right), \tag{49}$$

the fixed-k transition probability, maximized over all k values. Then, for example, if it is desired to keep $T_{\max} \leqslant 10^{-3}$, this can be accomplished by arranging to have $\left|\frac{v-w}{v+w}\right| > .96$.

5. Conclusion

In this paper, we have constructed explicit expressions for the position-space wavefunctions of the SSH model in the case of an initially localized particle, and examined what happens to them when the propagating wavefunction encounters a change in system parameters that discontinuously alters the system's winding number. Any mode hitting the interface between regions exhibits some reflection backward. Therefore transmissions across the boundary are suppressed, and if v and w are well-chosen they can be made arbitrarily small. It is well-known that localized edge states existing at boundaries between regions with different values of a topological invariant enjoy a form of protection against perturbations.

The results here imply that under some conditions a weaker form of (approximate) protection can be made to extend to states in the bulk regions: if a severe external perturbation to the Hamiltonian causes a change in winding number in some region, the wavefunction resists entering that region, and tends to stay in the unperturbed region of original winding number. Since this happens due to the change in a topological quantum number, it could be referred to as 'topologically-assisted suppression of transitions' of the bulk wavefunction. This effect has obvious applications, since it can be used to protect quantum information encoded in bulk wavefunctions against environment-induced errors. Such applications will be examined in detail elsewhere.

Acknowledgments

This research was supported by the National Science Foundation EFRI-ACQUIRE grant no. ECCS-1640968, AFOSR grant no. FA9550-18-1-0056, and by the Northrop Grumman NG Next.

Appendix A

In this appendix, we display two physical implementations of photonic quantum walks that can be used to simulate the SSH system.

In figure A1(a), a polarized photon undergoes a sequence of polarization rotations (implemented by half-wave plates, represented here by the red rectangles) and polarization-dependent translations (birefringent beam displacers, the yellow rectangles). After each step, a beam splitter (at each point where the lines split in the diagram) sends each incoming photon into a superposition of two outgoing spatial states. After N steps, the photon can be in any of N outgoing spatial modes. With each time step, the waveplates are arranged so that the photon has amplitudes to move both one step up and one step down (depending on polarization), so that, while the photons exhibit steady motion from left to right, they also exhibit a quantum walk in the vertical direction. By having the rotation angles alternate between two values in the vertical direction, the hopping amplitudes in the vertical direction also alternate, leading to SSH-type behavior [5, 8].

A second photonic implementation is shown in figure A2(b). Here, the basic building block (lower right) is the directionally-unbiased optical three-port [23, 24]. A photon entering any of the input ports can exit any of the three output ports, with amplitudes that can be controlled by altering the phase shifts introduced at the mirrors sitting at each vertex. By combining two of these three-ports with an additional phase shift ϕ (lower left), a two-port unit is formed with a pair of two-way input/output lines. We assume that these units are very small, essentially pointlike, compared to the distance between them. A photon entering one line of the two-port unit can be either transmitted through to the other side of the unit, or can be reflected back out to the incoming side; in other words, the unit forms a 1D scattering vertex for the photon. Over time, there will therefore be a quantum walk of the photon back and forth along the horizontal chain of vertex units. By varying ϕ, the amplitudes for reflection and transmission at each unit can be controlled. So by alternating between two values of ϕ on adjacent units in a chain (top of the figure), we can again arrive at alternating hopping amplitudes, producing a system that simulates an SSH model, with the lines between the vertex units representing the A and B subsites of the SSH model.

Appendix B

In this appendix, we construct exact solutions for the wavefunctions across the topological boundary.

Consider a right-moving state coming from the left and hitting the boundary between the two regions of different winding number. We will consider only states on the upper energy band; the negative energy band is similar. The full state of the system can be written in the form

$$|\Psi\rangle = |\psi_{k+}\rangle + r_k|\psi_{-k,+}\rangle + t_k|\psi'_{k+}\rangle + |\psi_{e,k}\rangle, \tag{B.1}$$

for $k > 0$ (right-moving incident wave), where the terms on the left represent, respectively, the incident, reflected, and transmitted state, as well as a localized edge state $|\psi_{e,k}\rangle$. We take the boundary to pass through the B subcell of the $n = 0$ site. Referring to figure B1, the transition between the two asymptotic solutions takes place over the span of the $n = 0$ and $n = 1$ sites, so the edge state may be expressed as

$$|\psi_{e,k}\rangle = \frac{1}{\sqrt{2N}}\left(a_0|A,0\rangle + b_0|B,0\rangle + a_1|A,1\rangle + b_1|B,1\rangle\right). \tag{B.2}$$

Using equations (36) and (37), the state may be written as

$$\begin{aligned}|\Psi\rangle = \frac{1}{\sqrt{2N}}\Bigg\{ &\sum_{-N+1}^{-1}\Big[e^{ikn}\left(|A,n\rangle + e^{-i(\theta_k - k/2)}|B,n\rangle\right) \\ &+ r_k e^{-ikn}\left(|A,n\rangle + e^{i(\theta_k - k/2)}|B,n\rangle\right)\Big] \\ &+ t_k\sum_{n=2}^{N} e^{ikn}\left(|A,n\rangle + e^{i(\theta_k + k/2)}|B,n\rangle\right) \\ &+ a_0|A,0\rangle + b_0|B,0\rangle + a_1|A,1\rangle + b_1|B,1\rangle\Bigg\}.\end{aligned} \tag{B.3}$$

Here, use has been made of the fact that the sign of θ_k changes as the boundary is crossed.

The Hamiltonian is of the form of equation (2) to the left of the boundary, while on the right it is of the same form with v and w interchanged. Keeping mind that the interchange of v and w also flips the sign of θ_k, this gives

$$\begin{aligned}\hat{H}|\Psi\rangle = \frac{1}{\sqrt{2N}}\Bigg\{ &\sum_{-N+1}^{-1}\Big[\left(e^{ikn} + r_k e^{-ikn}\right)\left(v|B,n\rangle + w|B,n-1\rangle\right) \\ &+ \left(e^{ikn}e^{-i(\theta_k - k/2)} + r_k e^{-ikn}e^{i(\theta_k - k/2)}\right)\left(v|A,n\rangle + w|A,n+1\rangle\right)\Big] \\ &+ t_k\sum_{n=2}^{N} e^{ikn}\left[\left(v|B,n-1\rangle + w|B,n\rangle\right)\right. \\ &\left.+ e^{i(\theta_k + k/2)}\left(v|A,n+1\rangle + w|A,n\rangle\right)\right] \\ &+ a_0\left(v|B,0\rangle + w|B,-1\rangle\right) + b_0\left(v|A,0\rangle + v|A,1\rangle\right) \\ &+ a_1\left(v|B,0\rangle + w|B,1\rangle\right) + b_1\left(w|A,1\rangle + v|A,2\rangle\right)\Bigg\}.\end{aligned} \tag{B.4}$$

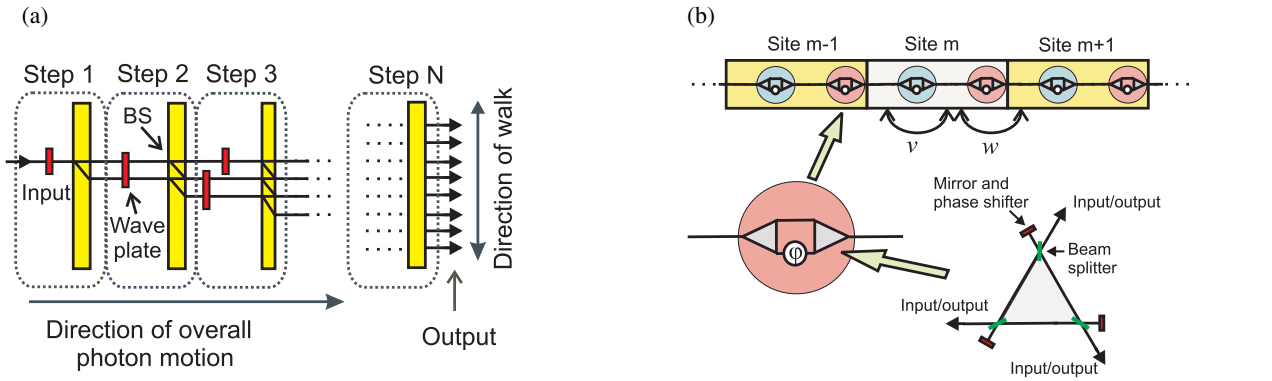

Figure A1. Two quantum walk architectures that can be used to create SSH-type behavior in a photonic system. (a) Alternating polization-dependent phase shifts produce a quantum walk in the vertical direction. (b) Pairs of directionally-unbiased multiports with alternating hopping amplitudes produce a quantum walk along the horizontal line.

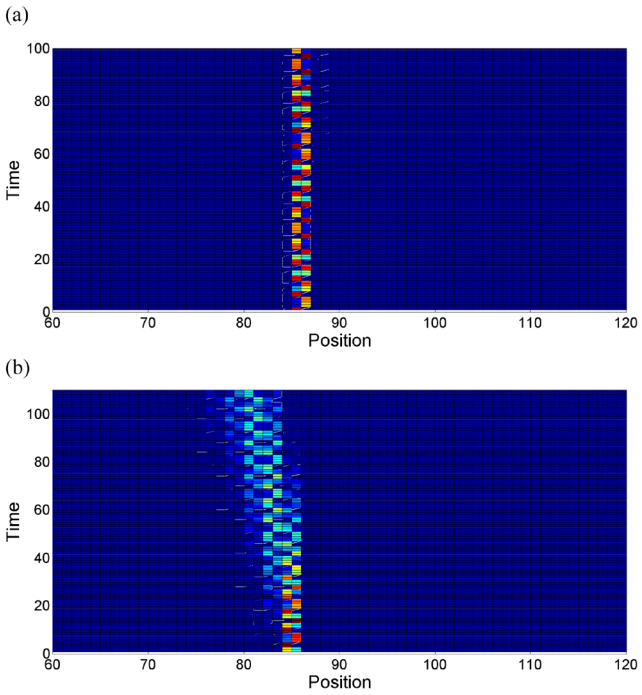

Figure A2. (a) When a photon is inserted at the boundary (the B subsite of cell 85 in the figure), the photon remains localized over time in the immediate vicinity of the boundary. (b) When inserted even one cell away from the boundary in either direction (cell 84 in the image shown), some amplitude remains at the boundary, but already most of it moves away in standard quantum walk fashion over time.

The state must satisfy $\hat{H}|\Psi\rangle = E_k|\Psi\rangle$. Equating terms of the same kind ($|A,1\rangle$, $|B,0\rangle$, etc) on each side leads to a set of equations that can be combined into a matrix equation of the form

$$M \cdot V = W, \tag{B.5}$$

where

$$M = \begin{pmatrix} 0 & v & -E_k & w & 0 & 0 \\ v & -E_k & v & 0 & 0 & 0 \\ 0 & 0 & w & -E_k & 0 & vy^4 \\ -E_k & v & 0 & 0 & \frac{wy}{x} & 0 \\ w & 0 & 0 & 0 & y(yv - \frac{E_k}{x}) & 0 \\ 0 & 0 & 0 & \frac{v}{y^2} & 0 & y(\frac{wy^2}{x} - E_k y) \end{pmatrix}, \tag{B.6}$$

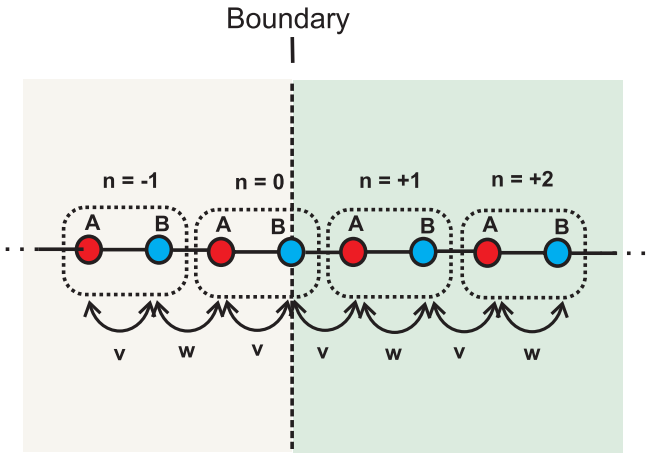

Figure B1. The boundary between distinct topological regions is taken to pass through the B subcell of site $n = 0$. When the boundary is crossed, the roles of v and w are interchanged.

and

$$V = \begin{pmatrix} a_0 \\ b_0 \\ a_1 \\ b_1 \\ r_k \\ t_k \end{pmatrix}, \qquad W = \begin{pmatrix} 0 \\ 0 \\ 0 \\ -wx/y \\ \frac{(E_k x - v/y)}{y} \\ 0 \end{pmatrix}. \tag{B.7}$$

Here, we have defined $x = \mathrm{e}^{-\mathrm{i}\theta_k}$ and $y = \mathrm{e}^{\mathrm{i}k/2}$. Making the further definition

$$\begin{aligned} D^{-1} = y^2((E^6 - v^4w^2 + E^2(v^2+w^2)(2v^2+w^2) \\ - E^4(3v^2+2w^2))x + (E^2 - v^2)vx^2)y \\ - E(E^2 - 2v^2 - w^2)((E^2 - w^2)w \\ + vw(E^4 + v^2w^2 - E^2(2v^2+w^2))xy^2), \end{aligned} \tag{B.8}$$

then the solutions of these equations are given by

$$\begin{aligned} a_0 = -D\,(vw\,((E_k^4 + v^4 - E_k^2(2v^2+w^2))x \\ + E_k w(-E_k^2 + v^2 + w^2)y)\,(x^2y^2 - 1)) \end{aligned} \tag{B.9}$$

$$\begin{aligned} b_0 = D\,(v^2w\,(-E_k^3 x + E_k(v^2+w^2)x \\ + E_k^2 wy - w^3 y)\,(x^2y^2 - 1)) \end{aligned} \tag{B.10}$$

$$a_1 = D(v^3 w(-E_k^2 x + v^2 x + E_k w y)(x^2 y^2 - 1)) \quad \text{(B.11)}$$

$$b_1 = D(v^3 w^2(-E_k x + w y)(x^2 y^2 - 1)) \quad \text{(B.12)}$$

$$\begin{aligned} r_k = Dy^{-1} \big(& x \left(E_k v(v^2 - E_k^2)(-E_k^2 + 2v^2 + w^2)x \right. \\ & - \left(E_k^6 x^2 + v^3 w^2 (w - v x^2) \right. \\ & + E_k^2 (2v^2 + w^2)(-vw + (v^2 + w^2)x^2) \\ & + E_k^4 (vw - (3v^2 + 2w^2)x^2)) \, y \\ & + E_k w (E_k^2 - w^2)(E_k^2 - 2v^2 - w^2) x y^2)) \end{aligned} \quad \text{(B.13)}$$

$$t_k = Dy^{-4} \left(v^4 w^2 x \left(1 - x^2 y^2 \right) \right). \quad \text{(B.14)}$$

Substituting these formulas into equations (B.1) and (B.2) gives an exact solution to the eigenvalue problem. The reflection and transmission coefficients of equations (B.13) and (B.14) were used to construct the plots of figures 5 and 6.

If the input is fed into the system at the boundary cell (figure A2(a)), the state remains over time in a superposition state with support on the two cells adjacent to the boundary point. This is consistent, for example, with the results of [25]. However, if the insertion point for the photon is even a single cell away from the boundary region, the state undergoes the usual ballistic quantum walk behavior, figure A2(b).

ORCID iDs

David S Simon https://orcid.org/0000-0003-4716-9244
Alexander V Sergienko https://orcid.org/0000-0003-0542-1405

References

[1] Su W P, Schrieffer J R and Heeger A J 1980 *Phys. Rev.* B **22** 2099
[2] Hasan M Z and Kane C L 2010 *Rev. Mod. Phys.* **82** 3045
[3] Asbóth J K, Oroszlány L and Pályi A P 2017 *A Short Course on Topological Insulators: Band Structure and Edge States in One and Two Dimensions* (Heidelberg: Springer)
[4] Kitagawa T, Rudner M S, Berg E and Demler E 2010 *Phys. Rev.* A **82** 033429
[5] Broome M A, Fedrizzi A, Lanyon B P, Kassal I, Aspuru-Guzik A and White A G 2010 *Phys. Rev. Lett.* **104** 153602
[6] Kitagawa T, Berg E, Rudner M and Demler E 2010 *Phys. Rev.* B **82** 235114
[7] Tarasinski B, Asbóth J K and Dahlhaus J P 2014 *Phys. Rev.* A **89** 042327
[8] Kitagawa T, Broome M A, Fedrizzi A, Rudner M S, Berg E, Kassal I, Aspuru-Guzik A, Demler E and White A G 2012 *Nat. Commun.* **3** 882
[9] Cardano F *et al* 2017 *Nat. Commun.* **8** 15516
[10] Simon D S, Fitzpatrick C A, Osawa S and Sergienko A V 2017 *Phys. Rev.* A **96** 013858
[11] Simon D S, Fitzpatrick C A, Osawa S and Sergienko A V 2017 *Phys. Rev.* A **95** 042109
[12] Simon D S, Osawa S and Sergienko A V 2018 *New J. Phys.* **20** 093032
[13] Meyer D A 1997 *Int. J. Mod. Phys.* **8** 717
[14] Kempe J 3002 *Contemp. Phys.* **44** 307
[15] Ambainis A 2003 *Int. J. Quantum Inf.* **1** 507
[16] Portugal R 2013 *Quantum Walks and Search Algorithms* (Berlin: Springer)
[17] Duncan C W, Öhberg P and Valiente M 2018 *Phys. Rev.* B **97** 195439
[18] Gu J and Sun K 2016 *Phys. Rev.* B **94** 125111
[19] Jackiw R and Rebbi C 1976 *Phys. Rev.* D **13** 3398
[20] Wannier G H 1937 *Phys. Rev.* **52** 191
[21] Kohn W 1959 *Phys. Rev.* **115** 809
[22] des Cloizeaux J 1963 *Phys. Rev.* **129** 554
[23] Simon D S, Fitzpatrick C A and Sergienko A V 2016 *Phys. Rev.* A **93** 043845
[24] Osawa S, Simon D S and Sergienko A V 2018 *Opt. Express* **26** 27201
[25] Naz E S G, Fulga I, Ma L, Schmidt O G and van den Brink J 2018 *Phys. Rev.* A **98** 033830